PHYSICAL REVIEW C **74**, 012801(R) (2006)

First experimental constraints on the interference of $\frac{3}{2}^+$ resonances in the ^{18}F(p, α)^{15}O reaction

K. Y. Chae,[1] D. W. Bardayan,[2] J. C. Blackmon,[2] D. Gregory,[3] M. W. Guidry,[1,2] M. S. Johnson,[4] R. L. Kozub,[3] R. J. Livesay,[5] Z. Ma,[1] C. D. Nesaraja,[1,2] S. D. Pain,[6] S. Paulauskas,[3] M. Porter-Peden,[5] J. F. Shriner Jr.,[3] N. Smith,[3] M. S. Smith,[2] and J. S. Thomas[6]

[1]*Department of Physics and Astronomy, University of Tennessee, Knoxville, Tennessee 37996, USA*
[2]*Physics Division, Oak Ridge National Laboratory, Oak Ridge, Tennessee 37831, USA*
[3]*Department of Physics, Tennessee Technological University, Cookeville, Tennessee 38505, USA*
[4]*Oak Ridge Associated Universities, Bldg 6008, P. O. Box 2008, Oak Ridge, Tennessee 37831, USA*
[5]*Department of Physics, Colorado School of Mines, Golden, Colorado 80401, USA*
[6]*Department of Physics and Astronomy, Rutgers University, Piscataway, New Jersey 08854, USA*

(Received 14 March 2006; published 10 July 2006)

The interference effects among $J^\pi = 3/2^+$ resonances in the ^{18}F + p system have not been previously measured. R-matrix calculations show that the cross sections above the $E_{\text{c.m.}} = 665$ keV resonance are sensitive to the interference between the $E_{\text{c.m.}} = 8$, 38, and 665 keV resonances. An excitation function for the ^{1}H(^{18}F,α)^{15}O reaction has been measured in the energy range of $E_{\text{c.m.}} = 663$–877 keV using radioactive ^{18}F beams at the Holifield Radioactive Ion Beam Facility (HRIBF). By comparing the observed cross sections with the R-matrix calculations, we provide the first experimental constraints on the interference. Upper limits on proton widths (Γ_p) of the $E_{\text{c.m.}} = 827$ and 842 keV resonances have been set as well.

DOI: 10.1103/PhysRevC.74.012801 PACS number(s): 27.20.+n, 25.40.Hs, 25.60.−t, 26.30.+k

The γ-ray emission from novae during the first several hours after the expansion is dominated by positron annihilation resulting from the beta decay of radioactive ^{18}F nuclei in the expanding envelope [1,2]. The decay of ^{18}F is the most important positron annihilation source during this time because of its relatively long half-life (110 min) and large production rate. ^{18}F is synthesized in novae via proton capture on ^{17}O or through the sequence ^{17}F(p, γ)^{18}Ne($e^+\nu_e$)^{18}F and is destroyed predominantly by the ^{18}F(p, α)^{15}O reaction [3]. Knowledge of the ^{18}F(p, α)^{15}O reaction is, therefore, very important for the estimation of the amount of ^{18}F that survives the explosion and thus the sensitivity of γ-ray telescopes to ^{18}F decay radiation.

Because of the importance of understanding the ^{18}F+p reactions, a number of studies of the $A = 19$ isobars have been made using stable and exotic beams [3–12]. These studies have substantially improved our understanding of the ^{18}F(p, α)^{15}O reaction. There are still, however, remaining questions to be answered. As an example, the interference among $J^\pi = 3/2^+$ resonances could not be taken into account in reaction rate calculations due to the lack of experimental knowledge about the relative signs of the effect. As described in Refs. [9,10], however, the interference has a significant effect on the reaction rate at nova temperatures. A recent calculation of the interference between the $E_{\text{c.m.}} = 38$- and 665-keV resonances reported by de Séréville *et al.* [9] found that the best fit to the data of Bardayan *et al.* [11] was obtained for constructive interference between the two resonances. That study was limited, however, in that the interference between all three low-lying $3/2^+$ resonances was not considered, and the calculations were constrained only by a single data point.

The goal of the present work was to study these interference effects by measuring the ^{18}F(p, α)^{15}O cross section off resonance. The cross sections on resonance are determined mostly by the properties of those resonances, while the cross sections off resonance are most sensitive to the interference. R-matrix calculations indicate that the cross section of the ^{18}F(p, α)^{15}O reaction at energies above the 665-keV resonance show a significant sensitivity to the interference of lower-lying 8-, 38-, and 665-keV resonances. The measurement of the ^{18}F(p, α)^{15}O reaction at energies above the 665-keV resonance (where the cross sections are larger) can thus be used to constrain the relative interference of the lower-lying levels.

The ^{18}F beam was produced at the ORNL Holifield Radioactive Ion Beam Facility (HRIBF) [13] using the Isotope Separator On-Line (ISOL) method. A beam of ^{4}He from the Oak Ridge Isochronous Cyclotron (ORIC) bombarded a thick HfO_2 target to produce ^{18}F atoms via ^{16}O(α,pn)^{18}F reaction [14]. The produced ^{18}F atoms were then mass analyzed and post accelerated by the tandem electrostatic accelerator to the appropriate energies for this experiment.

The ^{1}H(^{18}F,α)^{15}O excitation function was measured over the energy range $E_{\text{c.m.}} \simeq 663$–877 keV. A schematic diagram of the experimental setup is shown in Fig. 1. The ^{18}F beam ($\sim 10^5$ ^{18}F/s, ^{18}F/^{18}O ~ 0.04) was used to bombard a 70 μg/cm^2 polypropylene CH_2 target (5.5×10^{18} ^{1}H atoms/cm^2). 1 MeV steps were taken in bombarding energy ($\Delta E_{\text{c.m.}} \simeq 50$ keV) because the ^{18}F beam loses about 970 keV in the target at this energy.

Recoil α particles and ^{15}O ions from the ^{1}H(^{18}F,α)^{15}O reaction were detected in coincidence by two large area silicon detector arrays (SIDAR and MINI, respectively) as shown in Fig. 1. The SIDAR [8] was tilted forward 43° from the perpendicular to the beam axis in order to cover a large angular range ($29° \leqslant \theta_{\text{lab}} \leqslant 73°$), while the smaller annular detector (MINI) covers $11.5° \leqslant \theta_{\text{lab}} \leqslant 22.5°$. Scattered ^{18}F and ^{18}O ions were also continuously detected by a gas-filled ionization counter enabling a constant monitor of the beam composition.

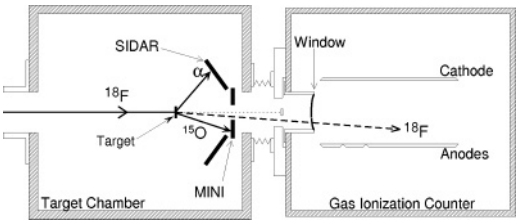

FIG. 1. A schematic diagram of the experimental setup is shown. A ^{18}F beam was used to bombard a 70 μg/cm^2 CH_2 target. The α particles and ^{15}O ions were detected in two silicon detector arrays, while scattered ^{18}F were detected in a gas-filled ionization counter.

The amount of ^{18}F deposited on target was determined from the amount of beam scattered from the carbon in the target and detected in the MINI detector using the measured ratio of ^{18}F/^{18}O in the beam and scaling, where appropriate, by the relative atomic numbers. The unscattered beam was stopped by a 1.5 cm disk which was put in front of the ion counter window to protect it from receiving the full beam intensity.

The ^{1}H(^{18}F,α)^{15}O and ^{1}H(^{18}O,α)^{15}N events were identified by reconstructing the total energy of detected particles in SIDAR and MINI (see Fig. 2). Inside of the gate shown in this figure, the intense events were from the ^{1}H(^{18}O,α)^{15}N reaction and the fainter line of events was from the ^{1}H(^{18}F,α)^{15}O reaction. The intense groups along the x- and y-axis are from elastic scattering. Owing to the different Q values for the reactions, the α particles from the ^{1}H(^{18}F,α)^{15}O reaction could be distinguished from the ^{1}H(^{18}O,α)^{15}N events.

To determine the number of ^{1}H(^{18}F,α)^{15}O events that were observed at a given energy, several selections ("cuts") to the entire data set were applied. The time between SIDAR and MINI events was measured via a time-to-amplitude converter (TAC), and the first cut was the requirement of an appropriate time coincidence. The next cut was in total energy—shown by the gate in Fig. 2. Finally, the coplanarity of the α particle and ^{15}O ion were checked (i.e., the α particle and ^{15}O ions should be detected opposite to each other in the array). With these conditions applied, the α angle was plotted versus its energy (Fig. 3) and the number of ^{18}F(p, α)^{15}O events summed.

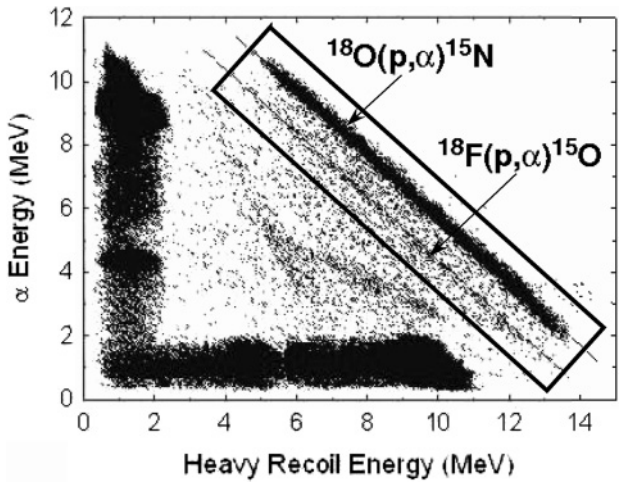

FIG. 2. α energy vs heavy recoil energy plot. Events from ^{1}H(^{18}F,α)^{15}O and ^{1}H(^{18}O,α)^{15}N are shown in the gate. In this gate, the intense line is from ^{1}H(^{18}O,α)^{15}N and the fainter line from ^{1}H(^{18}F,α)^{15}O. Strong elastic scattering groups lie along the x and y axes. ^{1}H(^{18}F,α)^{15}O events could be identified by their different Q values. Two dashed lines show the regions where the events from two reactions are expected from kinematics.

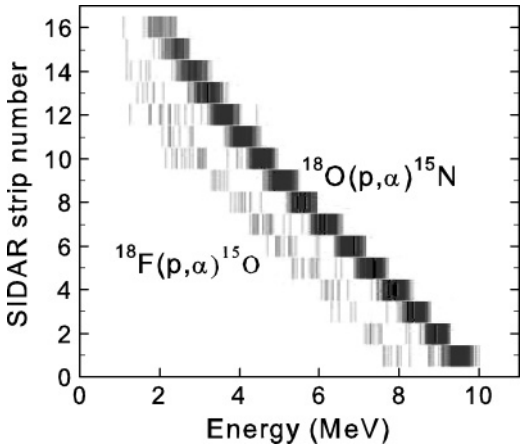

FIG. 3. SIDAR strip number vs energy plot for events with the correct total energy is shown. The ^{18}F(p, α)^{15}O and ^{18}O(p, α)^{15}N events are clearly visible. Here SIDAR strips 1–16 cover laboratory angles 29°–73°, respectively.

Even with all these conditions applied, there were still ^{18}O(p, α)^{15}N events which fell in the ^{18}F(p, α)^{15}O gate owing to the low purity of the beam. To estimate the number of contaminant events, we ran with a pure ^{18}O beam at each energy under identical conditions. This was done quickly by ending the cyclotron bombardment at the ISOL target with the ^{18}F component decaying quickly with a half-life on the order of the hold up time in the target (∼minutes) [14]. We then subtracted the estimated amount of contaminant events from those in the ^{18}F(p, α)^{15}O gate to obtain the number of events of interest. These pure ^{18}O beam runs were also useful for checking the beam current normalization since the ^{18}O(p, α)^{15}N cross section is well known [15].

The differential cross section in the center of mass system at each energy was calculated as

$$\left(\frac{d\sigma}{d\Omega}\right)_E = \frac{Y(E)}{IN\sum_s \Delta\Omega_s \epsilon_s}, \qquad (1)$$

where $Y(E)$ was the number of α particles identified from ^{1}H(^{18}F,α)^{15}O reaction, I was the number of ^{18}F ions incident on the target, N was the number of hydrogen atoms per unit area, $\Delta\Omega_s$ was the solid angle covered by a SIDAR strip in the center of mass system, and ϵ_s was the coincidence efficiency for detecting an α particle in that strip and the corresponding ^{15}O ion in the MINI detector. The beam current was determined from the number of scattered ^{18}F and ^{18}O ions detected in the MINI at $\theta_{\rm lab} = 12^\circ$ assuming Rutherford scattering, and the solid angle covered by each strip was obtained using a calibrated ^{244}Cm source which emits 5.8 MeV α particles. This measured solid angle agreed with geometric calculations within 3%. The coincidence efficiency of each strip was calculated from the known detector geometry and kinematics. The ^{18}F(p, α)^{15}O cross sections from our study are plotted in

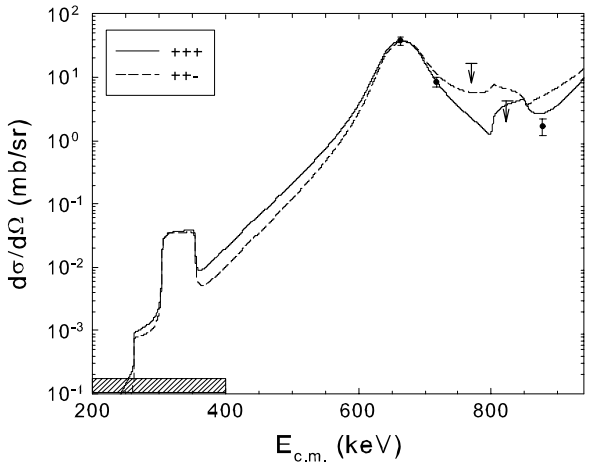

FIG. 4. The ^{18}F$(p,\alpha)^{15}$O excitation function is shown in the figure together with calculations from the *R*-matrix code MULTI. The theoretical cross section was calculated over the complete range of energies and then averaged over the energy loss in the target as well as over the angles covered by SIDAR ($56^\circ \leqslant \theta_{c.m.} \leqslant 138^\circ$) for direct comparison with the data. Two cases of the relative interference signs are shown for illustration (see text). Most effective energy range for novae is indicated by the shaded box.

Fig. 4. As a result of the ^{1}H(^{18}O,α)^{15}N cross section peaking at $E_{c.m.} = 789$ keV and the large ^{18}O contamination of the beam, only upper limits on the cross section were obtained at $E_{c.m.} = 770$ and 824 keV.

Although the relative normalization of the cross section data was well determined, determining the absolute normalization was not trivial mainly due to systematic effects such as the uncertainty in the number of hydrogen atoms in the target. This uncertainty was minimized by normalizing our cross sections to those from the well-known ^{1}H(^{18}O,α)^{15}N reaction which was simultaneously measured. The previously measured ^{1}H(^{18}O,α)^{15}N differential cross section [15] is uncertain by $\pm 15\%$ meaning that the absolute normalization of our work is also uncertain by that amount.

To study the interference effects on the cross section, the *R*-matrix code MULTI [16] was used along with the resonance parameters summarized in Table I. We took $\Gamma_p = 0.2$ keV for $E_r = 842$ keV resonance in order to obtain the best fit to the current data, which is consistent with the upper limit on the width (1.8 keV) found in Ref. [12]. To obtain the Γ_p value for $E_r = 842$ keV resonance, we reduced the width until the change in χ^2 value was negligible. While we use $\Gamma_p = 0.2$ keV in our calculations, any value of Γ_p smaller than this would also produce an equally good fit of our data. The theoretical cross section was calculated over the complete range of energies and then averaged over the energy loss in the target as well as over the angles covered by SIDAR for direct comparison with the data. For levels with the same J^π value, the astrophysical S-factor due to those levels can be taken from Eq. (XII. 5.15) of Lane and Thomas [17], and expressed as

$$S_{\text{tot}} = \left| \sum_j \pm \sqrt{S_j} e^{i\delta_j} \right|^2, \qquad (2)$$

TABLE I. Summary of resonance parameters used in calculation of ^{1}H(^{18}F,α)^{15}O cross section. All these parameters were taken from Refs. [10,12] and references therein. Note: The proton width for the 842 keV resonance in Ref. [12] is 0.9 ± 0.9 keV (see text).

E_r (keV)	J^π	Γ_p (keV)	Γ_α (keV)	Ref.
8	$3/2^+$	2.2×10^{-37}	0.5	[10]
26	$1/2^-$	1.1×10^{-20}	220.0	[10]
38	$3/2^+$	4.0×10^{-15}	4.0	[10]
287	$5/2^+$	1.2×10^{-5}	1.2	[10]
330	$3/2^-$	2.22×10^{-3}	2.7	[11]
450	$7/2^-$	1.6×10^{-5}	3.1	[12]
664.7	$3/2^+$	15.2	24.0	[8]
827	$3/2^+$	0.35	6.0	[12]
842	$1/2^+$	0.2	23.0	[12]
1009	$7/2^+$	27.0	71.0	[12]
1089	$5/2^+$	1.25	0.24	[12]
1122	$5/2^-$	10.0	21.0	[12]

where j is the resonance index, S_j is the S-factor from the resonance with index j, and δ_j is the phase [$\tan(\delta_j) = \Gamma/(2(E_j - E))$]. Each term in this sum can have either positive or negative signs [18]. This ambiguity results in the observed interference in the cross section. The relative signs of the terms can not be determined theoretically but only from comparison with the measured cross section.

We take as free parameters the signs of three resonance terms for the $E_{c.m.} = 8$, 38, and 665 keV resonances. The other $J^\pi = 3/2^+$ resonance at $E_{c.m.} = 827$ keV was not included because the effect from this resonance was small resulting from its small reduced width. The results show that four out of the eight possibilities ('plus' and 'minus' signs for each term) could be ruled out. The only combination of signs consistent with our data have the 665-keV resonance term as positive [i.e., (+++), (+−+), (−++), (−−+) where the signs in parenthesis represent the signs of the 8-, 38-, and 665-keV resonances, respectively, in the sum in Eq. (2)]. All four of these possibilities produce nearly identical cross sections above the 665-keV resonance. In Fig. 4, we show the clear rejection of the cases with a negative sign for the 665-keV resonance term. The signs of the other two resonances, $E_{c.m.} = 8$ and 38 keV, do not strongly affect the cross section above 665-keV. Interference effects from these resonances are, however, more important at the lower energy range ($E_{c.m.} \leqslant$ 600 keV) as shown in Fig. 5. Effects from higher-lying $3/2^+$ resonances (such as a mirror to the 9.204-MeV ^{19}F level) were also considered but found to be negligible. χ^2 values for the eight possible combinations are quantified in Table II.

New upper limits on the proton widths (Γ_p) of the $E_{c.m.} =$ 827 and 842 keV resonances have also been set. For a given set of resonance parameters, the upper limits on Γ_p were calculated at 90% confidence level from the χ^2 distribution. Upper limits were found to be $\Gamma_p \leqslant 1.17$ keV at $E_{c.m.} =$ 827 keV and $\Gamma_p \leqslant 1.65$ keV at $E_{c.m.} = 842$ keV. The upper limit at $E_{c.m.} = 842$ keV is consistent with the previously determined values from a ^{18}F$(p,p)^{18}$F measurement in Ref. [12], while the other upper limit is less stringent than the previous one.

TABLE II. χ^2 values for the eight possible combinations.

Combinations	χ^2
+++	4.00
−++	3.23
+−+	1.16
−−+	1.00
++−	72.19
−+−	38.45
+−−	40.67
−−−	48.04

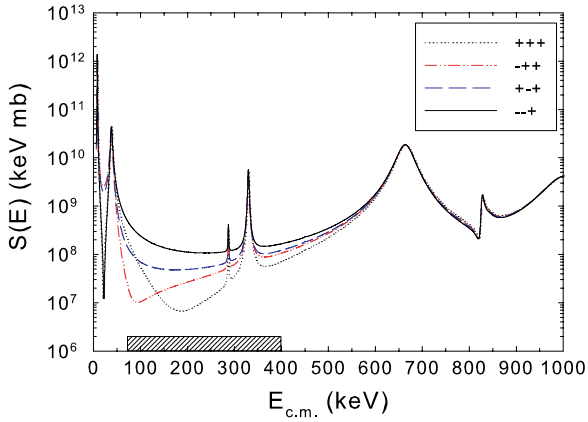

FIG. 5. (Color online) Astrophysical S-factor vs center of mass energy plots for four allowed possibilities. The signs of reduced widths for the $E_{c.m.} = 8$, 38, and 665 keV resonances are shown in the legend. The most effective energy range for novae is also indicated.

Calculations for the astrophysical ^{18}F$(p,\alpha)^{15}$O S-factor are shown in Fig. 5. Our measurements provide the first experimental constraints on the signs of the interference between $3/2^+$ resonances. There are still considerable uncertainties in the signs for the other resonances, but measurements of the cross section between the 330-keV and the 665-keV resonances along with this work would allow for a nearly complete characterization of the interference. This is illustrated in Fig. 5 showing the remaining possibilities for the S-factor depending on the interference signs for the 8- and 38-keV resonances.

To investigate how this uncertainty in interference propagates to uncertainties in ^{18}F production in novae, we have performed element synthesis calculations in the framework employed in the *Computational Infrastructure for Nuclear Astrophysics* [19]. Similar to Ref. [20], a nuclear reaction network [21] containing 169 isotopes from ^{1}H to ^{54}Cr was used with nuclear reaction rates from the REACLIB [22] database. Thermodynamic histories (time histories of the temperature and density) from one-dimensional hydrodynamic calculations were extracted for nova outbursts on a 1.35 $M_\odot$ ONeMg white dwarf [23]. Reaction rate variations in the ^{18}F$(p,\alpha)^{15}$O reaction do not appreciably change the nuclear energy generation, and thus this decoupling of nuclear and hydrodynamical effects is valid. The ejected envelope is divided into 28 zones, each with its own thermodynamic history. Separate reaction network calculations were carried out within each zone, and the final abundances determined by summing each zone's contribution to the total mass. We find that the uncertainty in the ^{18}F$(p,\alpha)^{15}$O reaction rate due to interference effects produces roughly a factor of 2 variation in the amount of ^{18}F produced in the calculation with the largest variation occurring in the innermost, hottest zone where a factor of 18 variation was produced.

In conclusion, the ^{18}F$(p,\alpha)^{15}$O reaction rate was uncertain partly because of the lack of experimental knowledge about the relative signs of the interference of three $3/2^+$ resonances. By measuring the ^{1}H(^{18}F,α)^{15}O cross sections in the energy range of $E_{c.m.} = 663$–877 keV using radioactive ^{18}F beams at the HRIBF, we provide the first experimental constraints on the interference effects. Our results show that the uncertainty in the reaction rate at the temperature range 0.3 GK $\leqslant T \leqslant$ 0.6 GK is reduced by up to 37% compared to previous work [10]. We also set new upper limits on proton widths at $E_{c.m.} =$ 827 keV ($\Gamma_p \leqslant$ 1.17 keV), and $E_{c.m.} = 842$ keV ($\Gamma_p \leqslant$ 1.65 keV).

Oak Ridge National Laboratory is managed by UT-Battelle, LLC, for the U.S. Department of Energy under contract DE-AC05-00OR22725. This work was also supported in part by the U.S. Department of Energy under Contract Nos. DE-FG02-96ER40955 and DE-FG02-96ER40990 with Tennessee Technological University, and DE-FG03-93ER40789 with the Colorado School of Mines.

[1] A. Coc, M. Hernanz, J. José, and J.-P. Thibaud, Astron. Astrophys. **357**, 561 (2000).
[2] M. Hernanz, J. José, A. Coc, J. Gómez-Gomar, and J. Isern, Astrophys. J. **526**, L97 (1999).
[3] S. Utku *et al.*, Phys. Rev. C **57**, 2731 (1998).
[4] R. Coszach *et al.*, Phys. Lett. **B353**, 184 (1995).
[5] K. E. Rehm *et al.*, Phys. Rev. C **53**, 1950 (1996).
[6] D. W. Bardayan *et al.*, Phys. Rev. C **62**, 042802(R) (2000).
[7] J.-S. Graulich *et al.*, Phys. Rev. C **63**, 011302(R) (2000).
[8] D. W. Bardayan *et al.*, Phys. Rev. C **63**, 065802 (2001).
[9] N. de Séréville, E. Berthoumieux, and A. Coc, Nucl. Phys. **A758**, 745c (2005).
[10] R. L. Kozub *et al.*, Phys. Rev. C **71**, 032801(R) (2005).
[11] D. W. Bardayan *et al.*, Phys. Rev. Lett. **89**, 262501 (2002).
[12] D. W. Bardayan, J. C. Blackmon, J. Gómez del Campo, R. L. Kozub, J. F. Liang, Z. Ma, L. Sahin, D. Shapira, and M. S. Smith, Phys. Rev. C **70**, 015804 (2004).
[13] D. W. Stracener, Nucl. Instrum. Methods Phys. Res. B **204**, 42 (2003).
[14] R. F. Welton *et al.*, Nucl. Phys. **A701**, 452c (2002).
[15] N. S. Christensen, F. Jensen, F. Besenbacher, and I. Stensgaard, Nucl. Instrum. Methods Phys. Res. B **51**, 97 (1990).

[16] R. O. Nelson, E. G. Bilpuch, and G. E. Mitchell, Nucl. Instrum. Methods Phys. Res. A **236**, 128 (1985).
[17] A. M. Lane and R. G. Thomas, Rev. Mod. Phys. **30**, 257 (1958).
[18] R. M. Freeman and G. S. Mani, Proc. Phys. Soc. (London) **85**, 267 (1965).
[19] Computational Infrastructure for Nuclear Astrophysics, http://www.nucastrodata.org.
[20] S. Parete-Koon, W. R. Hix, M. S. Smith, S. Starrfield, D. W. Bardayan, M. W. Guidry, and A. Mezzacappa, Astrophys. J. **598**, 1239 (2003).
[21] W. Raphael Hix and F.-K. Thielemann, J. Comput. Appl. Math. **109**, 321 (1999).
[22] T. Rauscher and F.-K. Thielemann, At. Data Nucl. Data Tables **79**, 47 (2001).
[23] S. Starrfield, J. W. Truran, M. C. Wiescher, and W. M. Sparks, Mon. Not. R. Astron. Soc. **296**, 502 (1998).